# FUNDAMENTAL STUDIES OF NEURAL STIMULATING ELECTRODES

**Eighth Quarterly Report**
**Covering Period May 29, 1996 to August 28, 1996**

**CONTRACT NO. N01-NS-4-2310**


S. F. Cogan
U. M. Twardoch
T. L. Rose
G. S. Jones
R. B. Jones
Y. P. Liu

EIC Laboratories, Inc.
111 Downey Street
Norwood, Massachusetts 02062


**Prepared for**

**National Institutes of Health**
**National Institute of Neurological Disorders and Stroke**
**Bethesda, Maryland 20892**

**November 11, 1996**

This QPR is being sent to you before it has been reviewed by the staff of the Neural Prosthesis Program.

## TABLE OF CONTENTS


| SECTION | | PAGE |
|---|---|---|
| 1 | INTRODUCTION AND SUMMARY | 5 |
| 2 | VOLTAMMETRIC STUDIES ON IR MICROELECTRODES | 6 |
| | 2.1 U. Michigan Ribbon-Cable Probe No. 1, Site 1 | 6 |
| 3 | ELECTROCHEMICAL IMPEDANCE SPECTROSCOPY | 12 |
| | 3.1 Overview of Impedance Spectroscopy | 12 |
| | 3.2 Experimental Set up for Impedance Spectroscopy | 13 |
| | 3.3 Results of Impedance Analysis | 15 |
| 4 | ELECTRODES WITH GRADED TI-IR INTERFACES | 23 |
| | 4.1 Preparation of Ti-Ir Bilayer and Alloy Films | 23 |
| | 4.2 Electrochemical Test Protocol | 25 |
| | 4.3 Activation of TiIr Alloys | 26 |
| 5 | FUTURE WORK | 27 |
| 6 | REFERENCES | 30 |

# LIST OF FIGURES


| Figure | | Page |
|---|---|---|
| 2-1 | Diagrammatic representation of sites and site identification on U. Michigan ribbon cable probe | 6 |
| 2-2 | Apparent capacitance of site 1 on U. Michigan ribbon-cable probe No. 1 at 200 V/s for the 23 scan rate studies | 9 |
| 2-3 | Comparison of voltammograms of electrode sites on U. Michigan ribbon cable No. 1 after 171 and 283 days of soaking | 11 |
| 3-1 | Nyquist plot of the impedance response of AIROF at 0.0V and 0.5V vs Ag/AgCl. The CSC of the AIROF is 47 mC/cm$^2$ | 16 |
| 3-2 | Nyquist plots of AIROF as a function of activation level at a fixed DC potential of 0.0 V vs Ag/AgCl | 16 |
| 3-3 | Equivalent circuit representation of process 1 based on the Huggins model | 17 |
| 3-4 | Ideal response of the equivalent circuit shown in Fig. 3-3 including the pseudo-capacitive process at low frequencies when finite diffusion length effects | 17 |
| 4-1 | Deposition rate of Ir and Ti as a function of power during DC sputtering | 24 |
| 4-2 | Cathodic charge storage capacity of TiIr alloys following pulsing in 0.3 M $Na_2HPO_4$ at 1 Hz between limits of -0.8 and 0.75V vs SCE | 26 |
| 4-3 | Cyclic voltammograms of TiIr alloys after 5,000 pulses in 0.3 M $Na_2HPO_4$. CV's in 0.3 M $Na_2HPO_4$ at 50 mV/s. | 28 |
| 4-4 | Comparison of TiIr alloys following 5,000 pulses in 0.3M $Na_2HPO_4$ between limits of -0.8V and 0.75V vs SCE (see Fig. 4-3). | 29 |

# LIST OF TABLES


| Table | | Page |
|---|---|---|
| 2-1 | Current measurements for the scan rate studies on site 1 of U. Michigan rhodium cable probe No. 1, site 1 | 8 |
| 3-1 | Parameter values and their relative errors from impedance spectroscopy measurements for the BAS Iridium disc electrode after 100 cycles of potential pulse activation | 20 |
| 3-2 | Parameter values and their relative errors from impedance spectroscopy measurements for the BAS Iridium disc electrode after 450 cycles of potential pulse activation | 20 |
| 3-3 | Parameter values and their relative errors from impedance spectroscopy measurements for the BAS Iridium disc electrode after 1150 cycles of potential pulse activation | 21 |
| 3-4 | Parameter values and their relative errors from impedance spectroscopy measurements for a U. Michigan probe, GSA = 4.08 x $10^{-7}$ $cm^2$, after 1150 cycles of potential pulse activation | 21 |
| 3-5 | Parameter values and their relative errors from impedance spectroscopy measurements for an HMRI Ir wire electrode after 1150 cycles of potential pulse activation | 22 |
| 3-6 | Ratio of thickness and square root of diffusion coefficient for various oxide thicknesses on different electrodes | 22 |
| 4-1 | Conditions for DC sputtering of Ti and Ir films | 24 |
| 4-2 | Nominal composition of TiIr alloys used in the activation study | 25 |

# I. INTRODUCTION AND SUMMARY

This report describes the work on NINDS Contract No. N01-NS-4-2310 during the period May 29, 1996 to August 28, 1996. As part of the Neural Prosthesis Program, the broad objectives of the present fundamental studies are: (1) to evaluate the electrochemical processes that occur at the electrode electrolyte interface during pulsing regiments characteristic of neural prosthetic applications; (2) to establish charge injection limits of stimulation electrode materials which avoid irreversible electrochemical reactions; (3) to develop an *in vitro* method, which can be applied *in vivo* for determining the electrochemical real area and stability of microelectrodes; (4) to develop new materials which can operate at high stimulation charge densities for microstimulation; and (5) to provide electrochemical and analytical support for other research activities in the Neural Prosthesis Program at NINDS.

During this reporting period, long term stability studies of a U. Michigan ribbon-cable probe No. 1, site 1 were continued for over 280 days. The apparent capacitance of the unactivated site, calculated from the current at 0.0V vs. Ag/AgCl in a 200 mV/s potential sweep, was used as an indicator of electrode stability. An increase in the capacitance after 100 days of soaking was observed. The capacitance increase was modest, from 0.5 nF to ~2.5 nF, and suggests that the metal/insulator seal, at this site, is stable. On day 217 of the soak test, the electrode was inadvertently allowed to dry out. The apparent capacitance measured subsequently has decreased to about the initial level. Cyclic voltammetry indicates that there is a significant amount of oxide on the charge injection site (~7 mC/cm$^2$ at 100 mV/s, even though the site was not deliberately activated.

A description of methods for applying and analyzing impedance spectroscopy for characterization of activated Ir is provided in this report. The methods have been applied in detail to a commercially available Ir microelectrode (BAS, 127 µm diameter Ir wire) and the effect of activation and electrode potential on the AC response determined. Preliminary comparison with microelectrodes for neural prosthesis research is also included. The impedance measurements can be analyzed to determine intrinsic material parameters for AIROF, such as the diffusion coefficient for the electroactive species.

Studies on graded Ti-Ir bilayers as a method for enhancing adhesion and preventing delamination of thin sputtered Ir films of overactivated, continued this quarter. Graded films were sputtered onto Si substrates by depositing Ti and Ir simultaneously while steadily increasing the Ir/Ti ratio throughout the layer to form the following structure:

Si | Ti (50 nm) | Ti-Ir (30-60 nm) | Ir (20-75 nm)

The films were masked with epoxy to form an electrode with a typical area of 0.01-0.02 $cm^2$. The Ir was subsequently activated in inorganic phosphate at pH 9.3. A detailed study of the effect of Ti-Ir alloy composition on activation was completed in the quarter and used to develop compositional profiles that optimize adhesion of the graded interface electrodes. Initial studies indicate a significant improvement in the mechanical stability of the electrodes with graded interfaces.

## 2. VOLTAMMETRIC STUDIES ON Ir MICROELECTRODES

### 2.1 U. Michigan Ribbon-Cable Probe No. 1, Site 1

During this quarter we continued studies of the long term stability of Ir sites on a probe with an integrated ribbon cable received from U. Michigan. The integrated ribbon cable allows long term soaking studies without any structures other than those fabricated on the wafer being exposed to the electrolyte solution, which avoids the previous problems with electrolyte penetration beneath the epoxy covering the contact pads. Figure 2.1 is a diagrammatic representation of the probe showing the numbering scheme for the electrode sites.

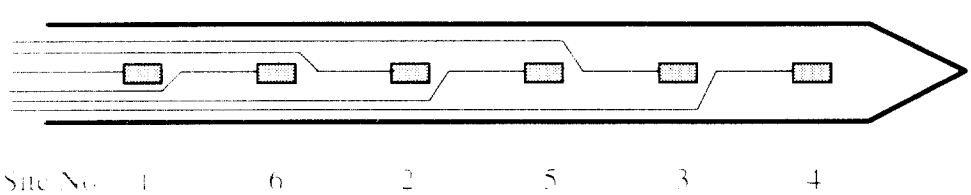


Figure 2.1 Diagrammatic representation of sites and site identification on U. Michigan ribbon-cable probe.

Apparent Capacitance Measurements. Measurements of the background residual currents on site [illegible] Michigan ribbon cable probe No. 1 were continued this quarter. Test procedures and results of the first 55 days of electrochemical testing were described in Quarterly Progress Report No. 5; those for days 55 through 108 were described in Quarterly Progress Report No. 6; and those for days 109 through 203 were described in Quarterly Report No. 7. This quarter we continued to monitor the electrode status during the long term soaking period from days 203 to 255.

Table 2-1 lists the background current obtained from the five studies performed this quarter along with the data from the eighteen studies conducted during the previous three quarters. The apparent capacitance, $C_{app}$, at 200 V/s, is plotted in Fig. 2-2 as a function of time. $C_{app}$ is calculated by dividing the current at 0.0V vs. Ag/AgCl by the scan rate, thus $C_{app} = Q/V = i/v$, where v is the scan rate.

The apparent capacitance at high sweep rates on a bare metal electrode should be directly proportional to the real electrochemical surface area. As discussed in Quarterly Progress Report No. 6, we have been using 25 μF/cm² real cm² as the proportionality constant based on literature values for measurements on Ir wire [1,2]. This value applies to an Ir surface that is perfectly smooth, i.e., has a roughness factor of 1, and the geometric and real surface areas are equal. For an electrode with a higher roughness factor, a larger proportionality constant must be used to obtain the geometric area of the electrode. Regardless of the absolute value of the proportionality constant, the increased current leading to the higher apparent capacitance between days 91 and 203 in Figure 2-2 would indicate an increase in area of a bare metal electrode. However the overall shape of the cyclic voltammograms did not change significantly over the soaking period, the current at the starting voltage was not anodic, and there was no "tilt" of the voltammogram, all indications of a "leak" between the metal and insulation layers.

Formation of oxide would explain the observed increase in the current through day 203 because the oxide has a specific capacitance many times that of the bare metal, even for very thin films. Cyclic voltammetry measurements made during this timeframe show that there was a significant amount of oxide on the electrode. On day 217, the electrolyte level was found below the tip of

the ribbon-cable probe, resulting in dehydration of the sites. The cell was filled with fresh 0.1M PBS solution and allowed to equilibrate for a few days in the hopes that any residual salts would dissolve without permanent damage to the sites. Prior to retesting, the cell was filled with a fresh solution of 0.1M PBS. A decrease in the apparent capacitance of the site was subsequently observed. The apparent capacitance values now closely approximate those measured in the first seven scan rate studies, and have not increased with additional soaking time. This observation is true for all the sweep rates studied.

Table 2.3 Current measurements for the scan rate studies on site 1 of U. Michigan ribbon-cable probe No. 1, Site 1

| Study | Days | (V/s)= | 0.05 | 10 | 20 | 50 | 100 | 200 |
|---|---|---|---|---|---|---|---|---|
| No. | Soaked | | | | Current (nA)* | | | |
| | 0 | | 0.096 | 6.2 | 11.0 | 26.8 | 45.5 | 79.5 |
| 2 | 8 | | 0.138 | 9.9 | 18.8 | 41.6 | 15 | 126 |
| 3 | 35 | | 0.142 | 11.8 | 21.4 | 45.0 | 79 | 134 |
| 4 | 52 | | 0.150 | 12.4 | 21.8 | 48.5 | 83.5 | 138 |
| 5 | 59 | | 0.144 | 12.3 | 21.4 | 46.0 | 78.5 | 130 |
| 6 | 70 | | 0.148 | 12.2 | 21.4 | 46.0 | 82.0 | 129 |
| 7 | 76 | | 0.156 | 11.8 | 21.2 | 46.0 | 82.5 | 127 |
| 8 | 91 | | 0.240 | 22.0 | 42.5 | 110 | 11 | 264 |
| 9 | 100 | | 0.226 | 33.0 | 58.0 | 128 | 230 | 365 |
| 10 | 108 | | 0.334 | 34.5 | 63.0 | 136 | 246 | 400 |
| | 135 | | 0.416 | 44.4 | 75.0 | 161 | 276 | 430 |
| 12 | 143 | | 0.446 | 50.5 | 86.0 | 181 | 318 | 508 |
| 13 | 150 | | 0.446 | 48.5 | 85.5 | 187 | 332 | 492 |
| 14 | 160 | | 0.555 | 60.5 | 104 | 222 | 380 | 605 |
| 15 | 164a | | 0.485 | 48.5 | 84.5 | 182 | 308 | 485 |
| 16 | 164b | | 0.610 | 53.5 | 95.0 | 200 | 344 | 510 |
| 17 | 171 | | 0.525 | 53.0 | 91.5 | 196 | 328 | 500 |
| 18 | 203 | | 0.500 | 48.0 | 80.0 | 168 | 268 | 415 |
| 19 | 220 | | 0.330 | 24.0 | 42.0 | 88.0 | 152 | 224 |
| 20 | 227 | | 0.255 | 17.0 | 30.5 | 62.0 | 108 | 185 |
| 21 | 233 | | 0.305 | 23.0 | 38.0 | 79.0 | 132 | 225 |
| 22 | 246 | | 0.20 | 16.0 | 27.0 | 8.00 | 98.0 | 170 |
| 23 | 272 | | 0.27 | 19.5 | 33.0 | 69.0 | 116 | 185 |

*Current at 0.0V vs. Ag/AgCl/3M NaCl measured from voltammogram taken in PBS.

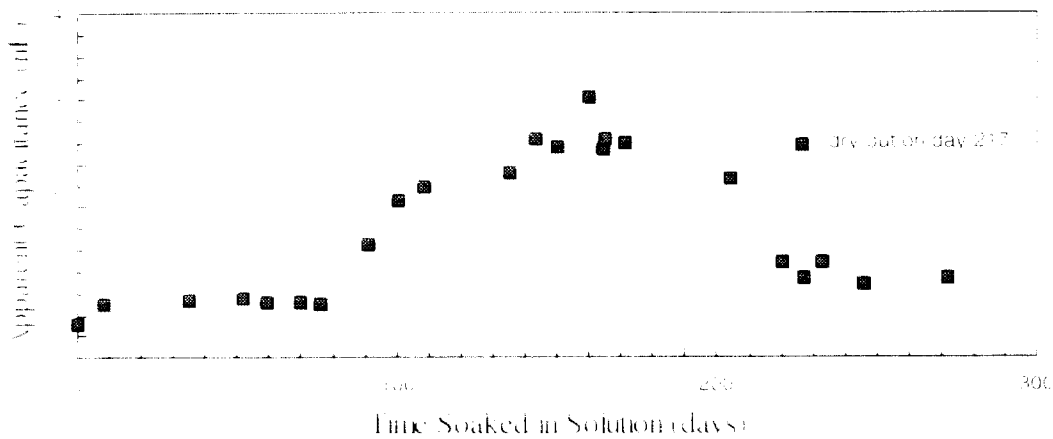


Figure 2.2 Apparent capacitance of site 1 on U. Michigan ribbon cable probe No. 1 at 200 V/s for the 2 s scan rate studies

Cyclic Voltammetry Analysis In order to minimize formation of iridium oxide by electrochemical activation, we have avoided as much as possible taking site 1 of ribbon No. 1 to very high anodic potentials. All of the initial scan rate studies done with Ru at the beginning of the soaking period and all the cyclic voltammogram measurements made to follow changes in the apparent capacitance were limited to potentials between -0.4 and +0.2V vs. Ag/AgCl. During LIS experiments the electrode was held at potentials in the range of -0.3 and +0.5V vs. Ag/AgCl. Activation of iridium oxide requires cycling of the electrode beyond certain threshold potential limits which depend somewhat on the electrolyte and growth conditions [1,2]. In our electrolyte at pH 7.3 the threshold of the anodic potential limit would be greater than 0.65V vs. Ag/AgCl. We expected, therefore, that there should be little, if any, formation of iridium oxide as a result of the electrochemical testing up to 203 days.

As discussed in Quarterly Report No. 5, one cyclic voltammogram was taken on each site on Ribbon 1 over the potential range from -0.4V to +0.6V vs. Ag/AgCl after 34 days of soaking. Another CV was taken on site 1 after 113 days of soaking (see figure 2.5 in QPR-6). The 34 day measurements showed that there was a small amount of oxide on some of the sites. The amount of oxide was largest on site 1 and decreased in the order of site 1, site 6, site 2 and site 5. This progression is not only the order of the sites ranked by distance from site 1, but also the order from the top of the probe closest to electrolyte atmosphere interface down into the solution. The

measurement on site 1 after 113 days showed about 50% increase in the current attributed to oxide on the electrode. As seen in Figure 2.2, the apparent capacitance measured at 200 V/s increased about a factor of three over this period.

In Quarterly Report No. 7 we showed cyclic voltammograms which were run at a wider potential window in order to evaluate the changes in the amount of oxide after 171 days of soaking the electrode. The potential range covered was from -0.56V to +0.85V vs. Ag/AgCl. This wider potential range provides more details of the electrochemistry of the oxide films. This quarter, the wider potential range was again used at a sweep rate of 100 mV/sec to evaluate the oxide films after 283 days. Cyclic voltammograms for each site taken between limits of -0.55 V and 0.85 V vs. Ag/AgCl on day 171 (solid lines) and day 283 (dashed lines) are compared in Fig. 2.3.

The results fall into three categories, each of which provides different information about the oxide. Site 3 continued to exhibit resistive behavior but with a large decrease in the overall current level. The CV also shows less "tilt" and anodic offset than the 171 day result. The CV of site 4 has similar characteristics, and has lost the small peaks associated with electrochemical reactions seen on day 171. There still appears to be a larger area of site 4 in contact with the electrolyte than site 3.

The CVs for sites 6, 2, and 5, listed in order from site 1, form another set of CVs with common properties. On day 171, one of the foremost features was that the current at 0.0V vs. Ag/AgCl on the positive going sweep for site 6 and site 2 had not changed since day 34 indicating little, if any, degradation of the seal between the insulation and the Ir metal. For site 5 the slightly higher current and small "tilt" indicated a slightly poorer, but still quite stable, insulator/metal seal. After 283 days however, the current value has changed for each of these three sites. Both site 6 and 5 now show a slight decrease, while site 2 shows an increase in the current at 0.0V vs. Ag/AgCl. The CVs for sites 6 and 5 also show a significant decrease in the electrochemical peaks in the anodic sweep associated with iridium oxide. The voltammogram for site 2 has become quite "tilted," and, although it retains electrochemical peaks indicative of iridium oxide, the site may be degrading.

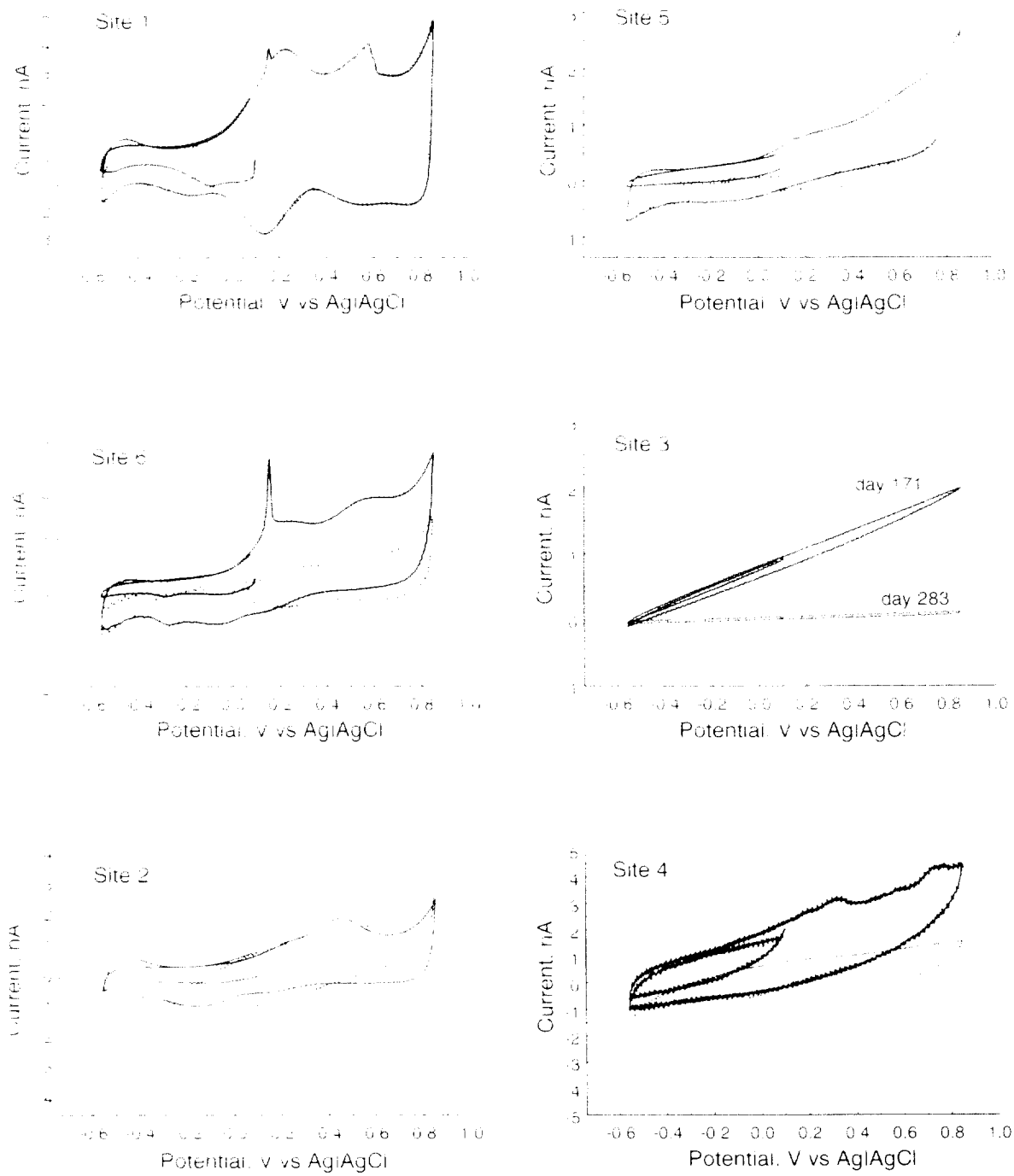


Figure 2-3 Voltammograms of electrode sites on U. Michigan ribbon cable No. 1 after 283 days of passive soaking (dashed line) and on day 171 (solid line). Measurements made in deaerated PBS at a scan rate of 0.1V/s.

The cyclic voltammogram for site 1 shows a large contribution from iridium oxide on both day 17 and day 283. Although there has been a decrease in the area under the electrochemical peaks associated with the iridium oxide, the cyclic voltammogram remains charge balanced and there are none of the typical indicators that there are problems with the insulator-metal seal. The major anodic and cathodic peaks have moved slightly anodic of those seen on day 171 to 0.27 V and 0.18 V vs. Ag/AgCl, respectively. These changes may all be due to the unexpected dehydration of the sites on day 217.

## 3. ELECTROCHEMICAL IMPEDANCE SPECTROSCOPY

### 3.1. Overview of Impedance Spectroscopy

In combination with other methods, ac impedance spectroscopy is a powerful technique for characterizing electrochemical systems. The response of an electrochemical system to ac perturbation can be measured in several ways. The classical impedance bridge approach displays the input and output signals simultaneously on an oscilloscope in the form of the Lissajous plot and the impedance is determined from the dimensions of that figure. Modern instruments employ phase sensitive detectors (PSD) that compare two sinusoidal signals yielding the phase difference between the signals as well as the ratio of the peak amplitudes.

In the bridge technique, both the dc and ac perturbation are applied across the cell - between the working and counter electrodes. The experimental cell consists of either three or two electrodes. In the three electrode arrangement, current is passed between the working and counter electrodes[a] and electrochemical potential of the working electrode monitored with a standard reference electrode. In a two electrode configuration, the working electrode is coupled with an electrode whose characteristics approach those of an ideal, non-polarizable electrode[b]. The electrochemical cell is designed so that the working electrode/electrolyte interface approximates an equipotential surface. The supporting electrolyte composition is chosen to minimize iR effects. This together with an appropriate choice of a large, essentially kinetically reversible counter electrode, allows considerable simplification of the mathematical analysis of the impedance characteristics of these

[a] The counter electrode is preferably an ideally polarized electrode, IPE.
[b] In aqueous systems a SCE with a large-area mercury electrode is used typically.

cells. The phase sensitive detection method then only determines the impedance of the working electrode, together with the solution between the working and the reference electrode.

In this quarter, we report on the application of steady state ac impedance measurements to iridium electrodes with different levels of activation. The methods have been applied in detail to a commercially available Ir microelectrode (BAS, 127 μm diameter Ir wire) and the effect of activation and electrode potential on the AC response determined.

### 3.2. Experimental Set-up for Impedance Spectroscopy

The electrolytes used to evaluate iridium "oxide" growth were: phosphate-buffered saline (PBS), 0.1 M $Na_2HPO_4$, $NaH_2PO_4$, 0.12 M NaCl, pH 7.2 and sodium mono-hydrogen phosphate, 0.3 M $Na_2HPO_4$, pH 9.1. The electrochemical cell (BAS, Bioanalytical Systems Inc.) was assembled in a 25 mL vial with Kel-F cell top. The cell was equipped with a gas bubbler and a large (1.5 $cm^2$) platinum spiral counter electrode. The reference electrode was a Microelectrode Inc., Ag | AgCl(s), Cl(3M KCl) || isolated from the main compartment by a salt bridge. All potentials are reported relative to this reference electrode. The potential of the electrode is 0.196 V vs. the normal hydrogen electrode (NHE) and -0.045 V vs. the saturated calomel electrode (SCE).

The iridium electrodes tested as the working electrode were: a) an iridium disk (BAS) with nominal diameter 127 μm and electrochemical surface area (ESA) 1.4 x $10^{-4}$ $cm^2$, b) an iridium disk which was fabricated by casting 1mm diameter wire in Epon resin 828, (ESA) 7.89 x $10^{-7}$ $cm^2$, c) a Michigan Ribbon-Cable Emory type probe with eight rectangular electrode sites of nominal geometric surface area (GSA) 4.08x$10^{-6}$ $cm^2$ and ESA of 5.3(±0.9) x $10^{-6}$ $cm^2$ for site 8; and, d) a Huntington Medical Research Institute electrode fabricated from annealed iridium wire [3,4] with a GSA of 4.75 x $10^{-4}$ $cm^2$ and ESA of 3.2(±1.7) x $10^{-5}$ $cm^2$. The electrochemical surface area of the electrodes was determined using multi-frequency cyclic voltammetric and chronoamperometric measurements for the diffusion controlled reduction of the ruthenium hexaaammine ions [5] and from ac impedance measurements in PBS solutions.

The electrochemical instrumentation was an Amel 551 potentiostat modulated by a PAR175 Universal Programmer. For current measurements below the minimum sensitivity level of the

Ame: 551 potentiostat, a BAS Model MF-2200 current amplifier was employed. Transients were recorded with a Bascom Turner 5120 microprocessor controlled recorder and stored on floppy disks for analysis. The electrochemical cell was inside a Faraday cage during all the electrochemical measurements. The cell was assembled and the solutions were de-oxygenated with a flow of argon before any electrochemical measurements were made.

The oxide films were formed on the iridium electrodes by applying consecutive sets of 50 square wave potential cycles between fixed cathodic and anodic limits. The potential limits for each electrolyte are -0.6 V to 0.8 V in PBS and -0.7V to 0.7V in 0.3 M $Na_2HPO_4$. After each 50 cycles cyclic voltammograms were acquired at scan rate 50 mV/s over the potential limits used in oxide formation. The charge associated with the oxidation/reduction of the surface films was determined by integration of the voltammograms.

The impedance instrumentation was an EG&G PAR 388 Electrochemical Impedance System. The apparatus comprises a Model 273 Potentiostat/Galvanostat and a Model 5210 Lock-in Amplifier. The system operates under computer control using PAR Software (V 2.92).

During the measurements, the working electrode was held at constant dc potential, and a 2 mV amplitude ac sinusoidal wave-form was applied. The unprocessed data acquired with the PAR 388 system are collected in the form of the real and the imaginary components of the voltage and the current. The frequency range selected for the measurements was 0.01 Hz to 100 kHz. The PAR 388 system uses a Fourier Transform (FT) technique for frequencies below 5 Hz. Twenty potential sine waves, each with different frequency and phase characteristics are digitally generated and mixed, are applied to the electrochemical cell. The system software deconvolutes the response into components for each of the twenty frequencies.

The dc potentials selected for impedance measurements in the electrolytes are listed in Table 3-1. The electrodes are held at the particular DC potential for 30 minutes to insure uniform composition within the oxide prior to the impedance measurement.

### 3.3. Results of Impedance Analysis

Plots of the experimental impedance data in the complex plane, i.e., plots of $-Z_{Im}(\omega)$ vs. $-Z_{Re}(\omega)$, for the iridium disk (BAS) electrode at potentials of 0.0 V and 0.5 V vs. Ag/AgCl and constant activation level of $4^{-7}$ mC/cm$^2$ are shown in Fig. 3-1. Similar data for AIROF at constant dc potential and different activation levels are shown in Fig. 3-2.

The experimental impedance data for a given system are analyzed by hypothesizing a plausible physical model to predict the impedance, $Z(\omega)$, mathematically or by using an empirical equivalent circuit approach to predict an impedance (symbolized by $Z_{ec}(\omega)$). In either case, the predicted parameters are compared with the experimental impedance, $Z_{ex}(\omega)$. Non Linear Least Squares Fitting techniques, NLLSF, provide the high precision fitting necessary in these approaches. Although electrochemically formed iridium "oxide" has been extensively studied, the mechanism of charge propagation is not understood and a mathematical description for these processes is unavailable. Glarum and Marshall demonstrated [6] that the electronic conductivity of electrochemical hydrous iridium "oxide" changed from less than $10^{-2}$ ohm$^{-1}$ cm$^{-2}$ for the reduced form to greater than $10^{2}$ ohm$^{-1}$ cm$^{-2}$ for the oxidized form. Thus, on this premise, the mechanism for charge transport in electrochemical iridium "oxides" is similar to that in the model for the electrochemical injection of metal atoms into transition metal oxides derived by Weppner and Huggins [7]. The process for AIROF is represented by:

$$IrO_2 + \gamma H^+ + \gamma e^- \Leftrightarrow IrOOH \qquad (1)$$

Process 1 is only intended to be a representation of the redox process and is obviously an oversimplification. The experimental impedance data reported here, however, for the iridium oxide and plotted in the complex plane exhibit features similar to those predicted by the Huggins model. The high frequency semicircle may be related to the parallel combination of the double layer capacitance, $C_{dl}$ of the substrate, and charge transfer resistance, $R_f$ of process 1 as shown in the equivalent circuit and corresponding ideal response shown in Figs. 3-3 and 3-4, respectively.

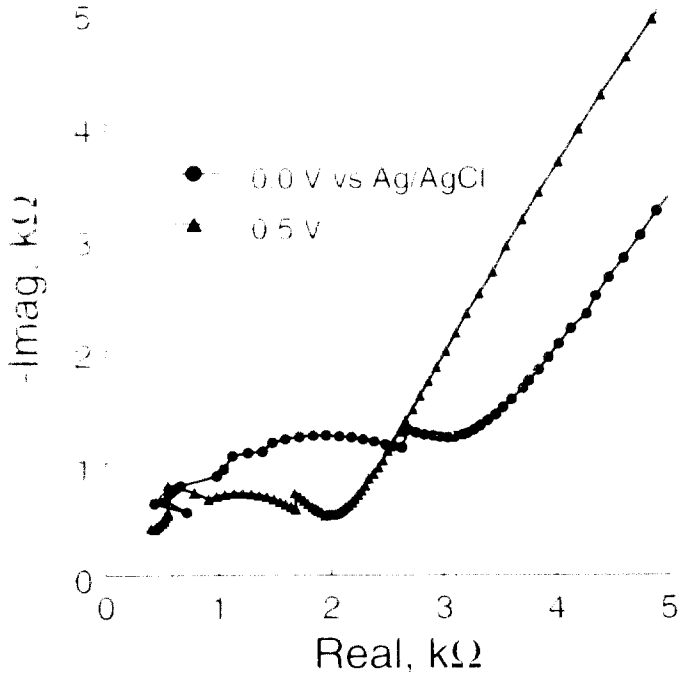


Figure 5-1 Nyquist plot of the impedance response of AIROE at 0.0V and 0.5V vs Ag/Ag/Cl. The CSC of the AIROE is 47 mC/cm

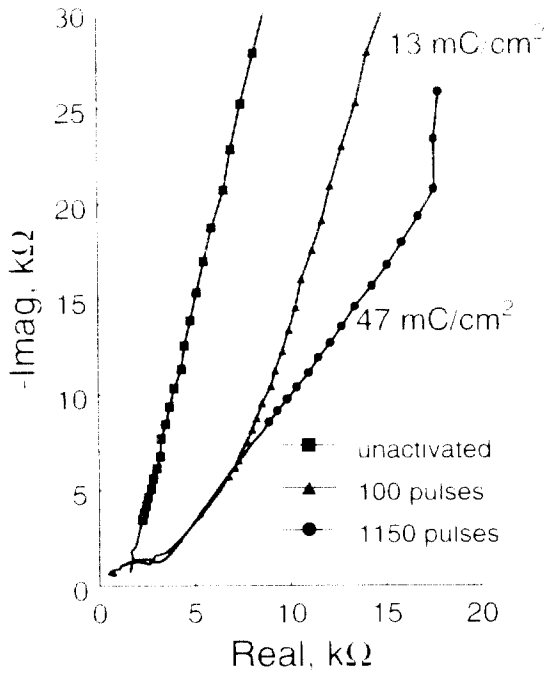


Figure 5-2 Nyquist plots of AIROE as a function of activation level at a fixed DC potential of 0.0V vs Ag/AgCl

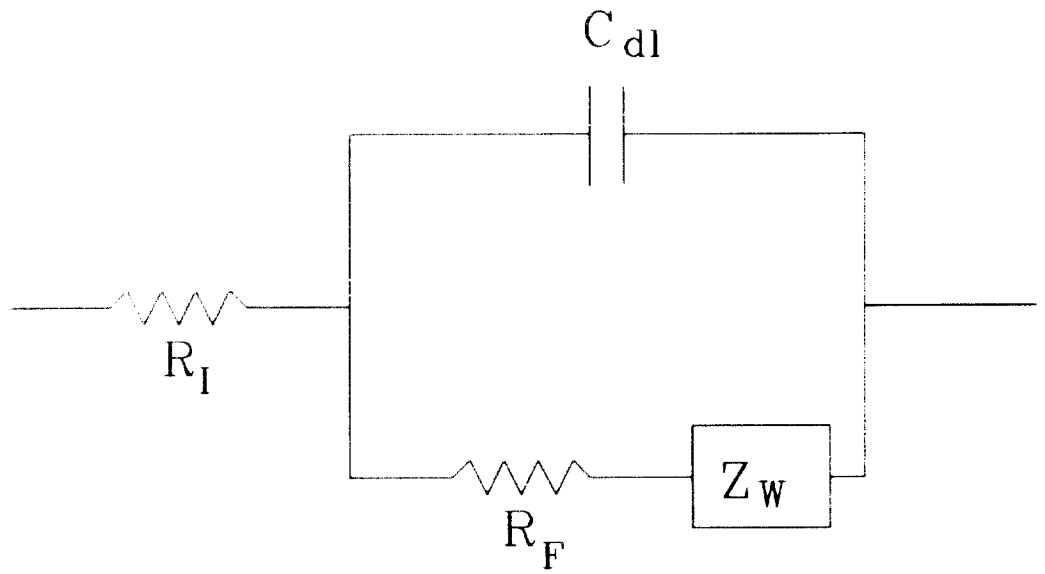


Figure 3-3 Equivalent circuit representation of process I based on the Huggins model. (See list of symbols on page 19)

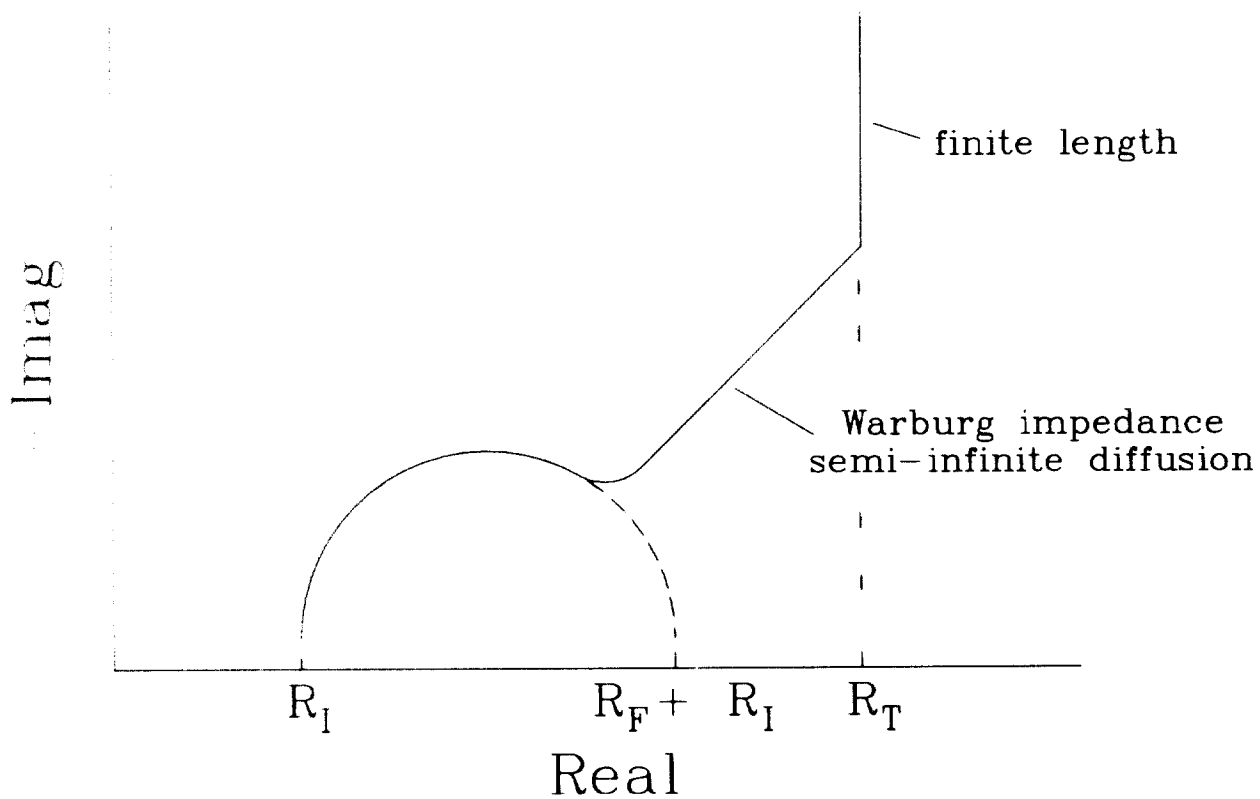


Figure 3-4 Ideal response of the equivalent circuit shown in Fig. 3-3 including the pseudocapacitive process at low frequencies when finite diffusion length effects dominate

As the frequency is decreased, a transition from charge transfer control to diffusion control (a straight line of 45° slope) is observed. Further decrease in the frequency results in an increase in the phase angle due to the onset of finite length effects. At "very" low frequencies (i.e. $\omega \leq 2D/l$) the resistance reaches its limiting value (vertical line).

$$R_{\infty} = R_{\Omega} + R_{c} + R_{\Omega} \qquad 2.$$

Where $R_{\Omega}$ is

$$R_{c} = \left[\frac{V_M}{F}\left(\frac{dE}{dy}\right)\right]\left[\frac{l}{3D}\right] \qquad 3.$$

and the imaginary part of the complex impedance, $Z_{Im}(\omega)$, is

$$Z_{Im}(\omega) = \frac{1}{\omega C_{\Omega}} \qquad 4.$$

where $C_{\Omega}$ is the electrochemical pseudocapacitance, associated with process 1. The term pseudocapacitance indicates that $C_{\Omega}$ is not an electrostatic capacitance but arises from a faradaic reaction which is given by

$$C_{\Omega} = \left[\frac{Fla}{V_M(dE/dy)}\right] \qquad 5.$$

$(dE/dy)$ is the rate of change of the AIROF potential with the compositional parameter y and is obtained from a very slow sweep rate cyclic voltammogram. For a given set of experimental data, preliminary values of parameters depicted in Figure 3-3 were obtained using the graphical procedure of the "EQUIVCRT"[8] Software, supplied by EG&G PARC. These parameters were used as initial values in a subsequent Non Linear Least Squares Fitting in which all the parameters in the equivalent circuit model were adjusted simultaneously. Typical data and the relative errors are shown in Tables 3-1 to 3-5.

The ratios of $(l/D^{1/2})$ were obtained from the values of $C_d$ and $R_f$. The values $(l/D^{1/2})$ are compared with the relevant $l/V_M$ values determined from voltammetric measurement of the total charge (Q) at the same activation level for the electrodes in Table 3-6 using the equation,

$$Q = \frac{F l a}{V_M} \qquad 6.$$

For a given AIROF film the magnitude of the limiting current density that can be obtained reversibly during charge injection is determined largely by the mass transport parameter $(l/D^{1/2})$, and the kinetic parameter $R_f$. Results presented here can not be taken as definitive measures to predict the limiting current density for the stimulation pulses, since the properties of the AIROF film are dependent on the activation method. The significance is that the diffusion coefficient and exchange current density, $I_o$, can be determined for any iridium oxide film using dynamic electrochemical techniques in conjunction with the steady-state ac technique. The important conclusion is that Huggins' model is applicable to analysis of ac impedance measurements for oxidation/reduction processes at iridium "oxide" films.

List of Symbols for Impedance Analysis

| | |
|---|---|
| $a$ | surface area of an electrode ($cm^2$) |
| $C_d$ | double layer capacitance (Farad) |
| $C_f$ | electrochemical pseudocapacitance (Farad) |
| $D$ | chemical diffusion coefficient ($cm^2s^{-1}$) |
| $E$ | potential of an electrode (V) |
| $F$ | Faraday's constant, 96485 ($C\ mol^{-1}$) |
| $i_o$ | exchange current (A) |
| $I_o$ | exchange current density ($Acm^{-2}$) |
| $l$ | thickness of the "oxide" (cm) |
| $Q$ | total charge (C) |
| $R$ | resistance (ohm) |
| $R_o$ | ohmic resistance (ohm) |
| $R_f$ | charge-transfer resistance (ohm) |
| $V_M$ | molar volume of $IrOOH_x$ ($cm^3mol^{-1}$) |
| $y$ | stoichiometric coefficient defined by $IrOOH_x$ |
| $Z$ | impedance (ohm) |
| $Z_{im}$ | imaginary part of the complex impedance (ohm) |
| $Z_w$ | Warburg impedance (ohm) |
| $\omega$ | angular frequency ($s^{-1}$) |

Table 3.1 Parameter values and their relative errors from impedance spectroscopy measurements for the BAS Iridium disc electrode, GSA = 1.27 x $10^{-4}$ $cm^2$, after 100 cycles of potential pulse activation in PBS where the pulse duration is 10 s at each potential limit.

| dc | $R_i$ | error | $R_F$ | error | $R_i$ | error | $C_d$ | error | $C_0$ | error |
|---|---|---|---|---|---|---|---|---|---|---|
| V | $10^{-3}$ Ω | % | $10^{-3}$ Ω | % | $10^{-4}$ Ω | % | $10^{-9}$ F | % | $10^{-7}$ F | % |
| 0.1 | 5.58 | 2.2 | 4.69 | 1.2 | 3.6 | | 1.56 | 1.3 | 5.94 | 4.5 |
| 0.0 | 4.83 | 7.3 | 2.10 | 3.8 | 2.3 | 18 | 2.55 | 4.7 | 2.47 | 6.0 |
| 0.1 | 4.05 | 5.0 | 1.38 | 3.9 | 2.0 | 14 | 3.94 | 4.9 | 5.84 | 5.4 |
| 0.2 | 3.30 | 5.9 | 1.30 | 2.7 | 2.4 | 26 | 3.86 | 4.0 | 7.35 | 6.1 |
| 0.3 | 3.27 | 6.4 | 1.21 | 3.7 | 2.3 | 14.5 | 3.88 | 4.5 | 4.20 | 5.8 |
| 0.4 | 3.96 | 5.4 | 1.29 | 4.3 | 2.3 | 14.6 | 4.39 | 4.8 | 4.08 | 5.0 |
| 0.5 | 3.31 | 6.2 | 1.28 | 3.6 | 2.1 | 11 | 3.96 | 4.4 | 4.98 | 3.9 |
| 0.7 | 3.49 | 7.2 | 1.28 | 3.4 | 2.3 | 9.7 | 4.92 | 7.2 | 4.88 | 3.7 |

Table 3.2 Parameter values and their relative errors from impedance spectroscopy measurements for the BAS Iridium disc electrode, GSA = 1.27 x$10^{-4}$ $cm^2$, after 450 cycles of potential pulse activation in PBS where the the pulse duration is 10 s at each potential limit.

| dc | $R_i$ | error | $R_F$ | error | $R_i$ | error | $C_d$ | error | $C_0$ | error |
|---|---|---|---|---|---|---|---|---|---|---|
| V | $10^{-3}$ Ω | % | $10^{-3}$ Ω | % | $10^{-4}$ Ω | % | $10^{-9}$ F | % | $10^{-7}$ F | % |
| 0.1 | 12.88 | 3.4 | 7.74 | 1.4 | 2.9 | 5.40 | 1.17 | 2.0 | 6.24 | 2.8 |
| 0.0 | 4.39 | 6.6 | 2.16 | 2.1 | 2.8 | 1.90 | 2.46 | 3.4 | 11.0 | 7.1 |
| 0.1 | 3.91 | 4.8 | 1.31 | 3.1 | 2.4 | 22.0 | 4.40 | 4.0 | 26.6 | 12.3 |
| 0.2 | 3.46 | 4.9 | 1.29 | 2.1 | 2.3 | 16.9 | 4.45 | 3.4 | 22.9 | 7.7 |
| 0.3 | 3.48 | 4.9 | 1.32 | 2.2 | 1.9 | 16.7 | 4.46 | 3.4 | 15.1 | 5.7 |
| 0.4 | 2.88 | | 1.34 | 3.8 | 2.7 | 9.80 | 3.99 | 4.1 | 12.9 | 5.0 |
| 0.5 | 3.02 | 6.2 | 1.33 | 3.2 | 2.9 | 13.2 | 4.19 | 3.9 | 16.0 | 6.2 |
| 0.7 | 3.04 | 6.2 | 1.31 | 3.2 | 2.9 | 1.00 | 4.21 | 4.0 | 14.7 | 7.7 |

Table 3-3 Parameter values and their relative errors from impedance spectroscopy measurements for the BAS Iridium disc electrode, GSA = 1.27 x $10^{-4}$ $cm^2$, after 1150 cycles of potential pulse activation in PBS where the the pulse duration is 10 s at each potential limit

| dc V | $R_i$ $10^{-4}\Omega$ | error % | $R_F$ $10^{-5}\Omega$ | error % | $R_f$ $10^{-4}\Omega$ | error % | $C_{di}$ $10^{-7}$F | error % | $C_\phi$ $10^{-7}$F | error % |
|---|---|---|---|---|---|---|---|---|---|---|
| 0 | 8.10 | 2.3 | 6.19 | 1.3 | 3.36 | 7.9 | 1.44 | 1.1 | 4.06 | 4.2 |
| 0.0 | 3.76 | 7.7 | 2.17 | 3.2 | 3.08 | 16.2 | 2.76 | 4.0 | 10.7 | 6.3 |
| 0 | 3.27 | 6.3 | 1.54 | 2.4 | 2.97 | 36.0 | 4.04 | 3.7 | 50.4 | 21.3 |
| 0.2 | 3.22 | 5.5 | 1.48 | 1.8 | 2.50 | 20.4 | 4.17 | 3.7 | 36.7 | 8.8 |
| 0.3 | 3.37 | 6.3 | 1.57 | 2.4 | 2.30 | 18.8 | 4.30 | 3.7 | 27.0 | 9.6 |
| 0.4 | 3.30 | 5.7 | 1.51 | 1.8 | 1.43 | 12.5 | 4.45 | 3.3 | 25.0 | 4.9 |
| 0.5 | 3.23 | 4.7 | 1.39 | 3.1 | 1.42 | 14.0 | 4.77 | 3.1 | 32.6 | 6.2 |
| 0.7 | 3.25 | 4.2 | 1.35 | 1.6 | 1.47 | 16.4 | 4.81 | 2.8 | 30.4 | 7.0 |

Table 3-4 Parameter values and their relative errors from impedance spectroscopy measurements for U. Michigan probe (R63-S8) electrode, GSA = 4.08 x $10^{-6}$ $cm^2$, after 1150 cycles of potential pulse activation in PBS where the the pulse duration is 10 s at each potential limit.

| dc V | $R_i$ $10^{-4}\Omega$ | error % | $R_F$ $10^{-4}\Omega$ | error % | $R_f$ $10^{-5}\Omega$ | error % | $C_{di}$ $10^{-10}$F | error % | $C_\phi$ $10^{-7}$F | error % |
|---|---|---|---|---|---|---|---|---|---|---|
| 0.0 | 0.11 | 2.8 | 0.24 | 1.5 | 0.22 | 20 | 0.24 | 3.0 | 0.03 | 15 |
| 0.20 | 2.12 | 7.2 | 3.00 | 4.5 | 9.79 | 36 | 2.35 | 9.8 | 0.16 | 21 |
| 0.30 | 1.66 | 12 | 3.13 | 5.7 | 1.05 | 51 | 1.94 | 12 | 0.17 | 21 |
| 0.40 | 1.14 | 24 | 3.18 | 73 | 3.74 | 26 | 1.67 | 17 | 0.10 | 7.8 |
| 0.50 | 1.30 | 49 | 2.55 | 23 | 3.76 | 26 | 1.99 | 48 | 0.12 | 9.0 |
| 0.70 | 1.74 | 21 | 2.13 | 15 | 3.64 | 20 | 3.10 | 34 | 0.10 | 5.4 |

Table 5.5 Parameter values and their relative errors from impedance spectroscopy measurements for an HMRE Ir wire electrode (F-19), GSA = 4.75 x $10^{-6}$ $cm^2$, after ~250 cycles of potential pulse activation in PBS where the the pulse duration is 10 s at each potential limit

| dc, V | $R_s$, $10^{-3}$ Ω | error, % | $R_p$, $10^{-3}$ Ω | error, % | $R_c$, $10^{-3}$ Ω | error, % | $C_p$, $10^{-1}$ F | error, % | $C_b$, $10^{-1}$ F | error, % |
|---|---|---|---|---|---|---|---|---|---|---|
| -0.1 | 0.27 | 11.6 | 8.32 | 4.5 | 7.1 | 8.3 | 2.59 | 3.3 | 0.43 | 7.3 |
| 0.0 | 0.33 | 6.5 | 2.83 | 1.9 | 2.4 | 6.4 | 3.74 | 2.5 | 2.61 | 3.6 |
| 0.2 | 0.37 | 2.6 | 0.67 | 1.1 | 0.12 | 25 | 11.2 | 2.7 | 8.17 | 10.8 |
| 0.3 | 0.35 | 2.0 | 0.59 | 0.97 | 0.61 | 15.3 | 12.6 | 1.5 | 3.48 | 5.3 |
| 0.4 | 0.12 | 2.1 | 0.49 | 1.0 | 0.35 | 9.4 | 15.3 | 1.5 | 2.86 | 5.4 |
| 0.7 | 0.88 | 2.7 | 0.28 | 1.4 | 0.26 | 19.5 | 23.6 | 2.3 | 3.37 | 6.3 |

Table 5.6 Ratio of thickness and square root of diffusion coefficient for various oxide thicknesses on different electrodes

| | Electrode Description | | | | |
|---|---|---|---|---|---|
| | **BAS** | **BAS** | **BAS** | **R63-S8** | **F-19** |
| Charge, mC/cm² | 13.0 | 30.2 | 47.4 | 48.1 | 59.0 |
| $\Theta/V_{sp}$, mol/cm² | 1.4E-7 | 3.1E-7 | 4.9E-7 | 5.0E-7 | 6.1E-7 |
| **dc, [V]** | **$(l/D^{1/2})$, $s^{1/2}$** | | | | |
| **-0.1** | 0.23 | | 0.21 | - | 0.29 |
| **0.0** | 0.12 | 0.29 | 0.40 | 0.41 | 0.41 |
| **0.1** | 0.18 | 0.42 | 0.65 | - | 0.17 |
| **0.2** | 0.22 | 0.38 | 0.51 | 0.48 | 0.20 |
| **0.3** | 0.17 | 0.28 | 0.41 | - | 0.20 |
| **0.4** | 0.18 | 0.31 | 0.31 | 0.32 | 0.16 |
| **0.5** | 0.17 | 0.36 | 0.35 | 0.29 | - |
| **0.7** | 0.18 | 0.35 | 0.34 | 0.32 | 0.15 |

# 4. ELECTRODES WITH GRADED Ti-Ir INTERFACES

In the previous quarter we began studies of fabrication procedures to permit stimulation at high charge densities by looking at methods for enhancing the adhesion and mechanical stability of electrode materials sputtered onto conductive substrates. The work focused on Ti-Ir electrodes deposited with discrete and compositionally graded interfaces. The compositional grading is intended to prevent delamination of AIROF should the Ir electrode be entirely consumed in the activation process. As observed previously (Quarterly Report No. 7), the increase in volume when Ir is electrochemically activated to form AIROF can be at least a factor of six. The strain associated with this volume change cannot be accommodated at a discrete Ti-Ir interface and the AIROF delaminates.

Initial studies compared discrete and graded interface electrodes by evaluating changes in cyclic voltammetry during potential pulsing between limits designed to deliberately overactivate the Ir. Some evidence for improved adhesion was obtained from a factor of 3 increase in the number of pulses required to delaminate graded interface AIROF and from EDS compositional analysis of fatigued electrodes. The results were not conclusive, however, and Auger depth profiling showed that the width of the graded interface was much narrower than intended. In the current reporting period, a series of TiIr alloys were prepared by sputtering and their activation evaluated, with the objective of, at least qualitatively, determining the activation volume change as a function of alloy composition. From these data and a more detailed knowledge of the Ti and Ir deposition rates, a more optimized graded interface electrode is being developed.

## 4.1. Preparation of Ti-Ir Bilayer and Alloy Films

The Ti and Ir are deposited by DC sputtering using a multitarget apparatus that allows near-simultaneous sputtering from independently controllable sputtering guns. The apparatus was described in QPR No. 7. Alloy films are obtained by co-sputtering from pure Ir and Ti targets. The composition of the films is controlled by adjusting the power to the sputtering guns and rotating the substrates under the targets at a sufficiently high rate that a homogeneous film is formed. Compositionally graded Ti-Ir interfaces are obtained by incrementing and decrementing the power to the individual sputter guns during deposition while maintaining a constant total

sputtering current or power. The deposition rates of the Ti and Ir determined, as a function of sputtering power, are shown in Fig. 4.1. The rates were determined from the thickness of the films measured with a surface profilometer and corroborated by SEM measurements of fracture cross sections. The rates are close to linear over the 25-100 watt power range investigated. The composition of the films was estimated from the deposition rates using the assumption that individual films are deposited at their bulk metal densities. Using constant power control during sputtering is a departure from the constant current mode used for the previous Ti and Ir depositions (QPR No. 5). The relationship between sputtering power and film thickness for the Ti and Ir appears slightly more linear than sputtering current versus film thickness. The deposition parameters, sputtering current and target voltage, are very similar for these modes and no difference in film properties is expected. The deposition conditions are detailed in Table 4.1.

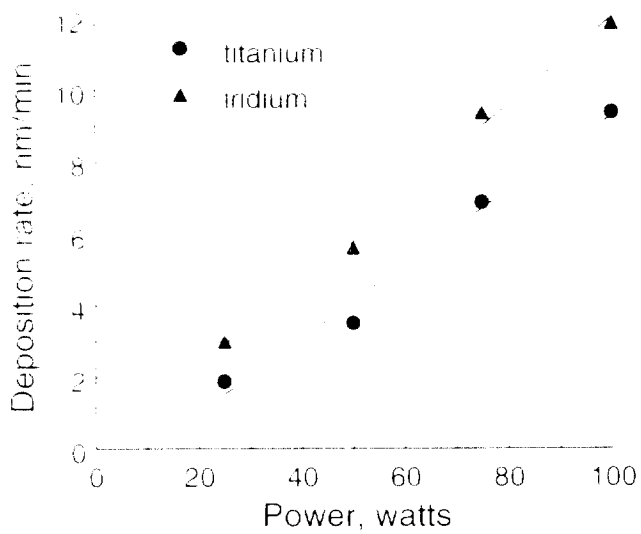


Figure 4.1 Deposition rate of Ir and Ti as a function of power during DC sputtering.

Table 4.1 Conditions for DC sputtering of Ti and Ir films.

| | |
|---|---|
| Base pressure | 2.0 x 10$^{-6}$ torr |
| Sputter gas and flow rate | Ar, 10 sccm |
| Sputtering pressure | 10 millitorr |
| Power | 25-100 watts |
| Target-to-substrate distance | 6.2 cm |
| Temperature | uncontrolled, near ambient |

For both the alloy and graded interface films, the substrates were polished, p-type Si used in the as-received condition without further cleaning. A 50–75 nm Ti adhesion layer was deposited on the Si prior to deposition of the Ir and alloy films. The composition and film thicknesses of the alloys investigated in the current reporting period are listed in Table 4-2.

Table 4-2. Nominal composition of IrTi alloys used in the activation study

| Composition[a] | Ir | | Ti | | Adhesion layer | Total film | Alloy film |
|---|---|---|---|---|---|---|---|
| at. % | power | thickness | power | thickness | thickness, nm | thickness, nm[b] | nm[c] |
| 100 | 100 W | 95 nm | | 0 nm | 75 | 170 | 95 |
| 75 | 80 W | 114 nm | 42 W | 58 nm | 50 | 180 | 130 |
| 52 | 85 W | 84 nm | 100 W | 78 nm | 47 | 165 | 118 |
| 45 | 42 W | 60 nm | 82 W | 90 nm | 50 | 160 | 110 |
| 35 | 32 W | 45 nm | 94 W | 105 nm | 50 | 145 | 95 |
| 28 | 26 W | 36 nm | 100 W | 115 nm | 50 | 140 | 94 |

[a] Composition calculated from the known deposition rates of the Ti and Ir assuming the metals are deposited at their bulk densities.

[b] Adhesion layer plus alloy film thickness measured with a Dektak surface profilometer.

[c] Calculated by subtracting the adhesion layer thickness from the total film thickness.

The alloy film thickness reported in Table 4-2 is less than that obtained by adding the expected film thickness of the individual Ir and Ti films. The difference becomes more pronounced with increasing Ti concentration in the alloy indicating a higher molar volume for the alloys. X-ray diffraction of the 100% Ir film showed a strong (111) preferred crystallographic orientation. The alloy films were also crystalline with diffraction spectra similar to the 100% Ir film and no clear indication for the formation of any of the phases in the Ir–Ti binary, such as $Ir_3Ti$, α-IrTi, or $Ti_3Ir$, was obtained.

## 4.2. Electrochemical Test Protocol

Alloy electrodes with an area of ~0.01–0.02 $cm^2$ were made by masking an approximately circular area of the sputtered films with epoxy. A quantitative measure of the area was then obtained using a digital camera with image analysis software. The electrodes were activated by pulsing in 0.5M $Na_2HPO_4$ (pH 9.2) using 1 Hz square pulses (0.5 s at each potential limit) between −0.8 and 0.75V vs. SCE. Cyclic voltammograms were taken periodically during

activation using a 50 mV/s triangular waveform between the activation potential limits. The charge storage capacity (CSC) of the AIROF was measured by integrating the cathodic or anodic current during each half cycle of the CV. The electrolyte was used without Ar sparging and therefore contains oxygen.

### 4.3. Activation of TiIr Alloys

The charge capacity as a function of the number of activation pulses is shown in Fig. 3.2 for the TiIr alloys. The 100% Ir alloys activate to a cathodic CSC of ~18 mC/cm$^2$ after 5,000 pulses as did the 79% Ir alloy. For lower Ir concentrations, the CSC decreased, with only very slight activation apparent after 5,000 pulses in the 35% Ir alloy and no activation in the 28% Ir alloy. Intermediate levels of activation were obtained with the 45% and 56% alloys.

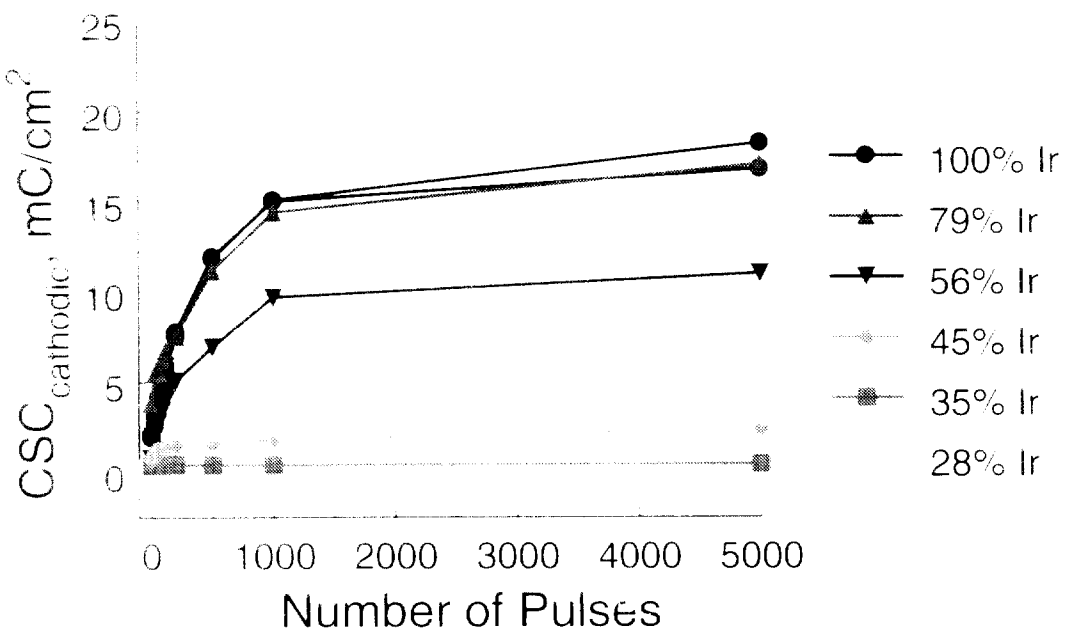


Figure 4-2 Cathodic charge storage capacity of TiIr alloys following pulsing in 0.3 M $Na_2HPO_4$ at 1 Hz between limits of -0.8 and 0.75 V vs SCE.

Cyclic voltammograms of the alloys after 5,000 activation pulses are shown in Fig. 4-3. The 28% Ir CV shows no evidence of activation and is similar to that obtained with 100% Ti films. The current is due primarily to double-layer charging with a slight indication of hydrogen

adsorption at the negative potential limit. The first indication of the $Ir^{3+}/Ir^{4+}$ redox couple is apparent in the 35% Ir CV from the peaks at -0.1 V and 0.1 V vs SCE. The higher Ir content also results in an increase in the hydrogen adsorption reaction. At 45% Ir, the CV acquires the familiar shape of AIROF with pronounced $Ir^{3+}/Ir^{4+}$ redox waves at -0.1/0.0 V and 0.33/0.4 V vs SCE. The cathodic CSC of the alloy is still quite low, ~4.5 mC/cm², and hydrogen adsorption/desorption reactions are apparent at potentials more negative than -0.45 V SCE. The 56% Ir alloy activates to a cathodic CSC of 12 mC/cm². The primary cathodic and anodic $Ir^{3+}/Ir^{4+}$ redox peaks occur at -0.17 V and 0.07 V vs SCE, respectively. The slight negative and positive displacements of the cathodic and anodic peaks, compared with the 45% Ir film, are probably due to increased iR effects in the thicker oxide layer. The cathodic CSC's of the 79% and 100% Ir films were similar, ~17-18 mC/cm². For comparison, the CV's of the pulsed alloys are compared in Fig. 4-4 on the same current density scale.

Pulsed alloy films are now being examined by SEM in an effort to determine the volume change on activation of the TiIr alloys. The thickness of the AIROF is being measured in two ways. If the TiIr film can be activated to the point that delamination occurs, the AIROF film is collected from the electrolyte and dried. It is then straightforward to obtain a thickness in the SEM. For those films that do not delaminate, the activated electrodes are fractured and examined in cross-section. A combination of secondary and backscatter images are used in an effort to differentiate between the AIROF and the unreacted Ir. Initial results indicate that alloys with greater than ~70 a/o Ir activate with a volume increase of 6, while little or no activation can be observed for alloys with less than ~40 a/o. The composition range over which TiIr interface should be graded is therefore 40-70 a/o.

## 5. FUTURE WORK

A more detailed analysis of activation protocols is planned for the succeeding quarter. We are currently evaluating the effect of pulse duration, potential limits and electrolyte (PBS or 0.3M $Na_2HPO_4$) on the activation of Ir and using cyclic voltammetry and impedance spectroscopy to characterize the AIROF. Atomic force microscopy is also being used to characterize the surface of the AIROF to develop a quantitative measure of surface roughness and provide general topographical information.

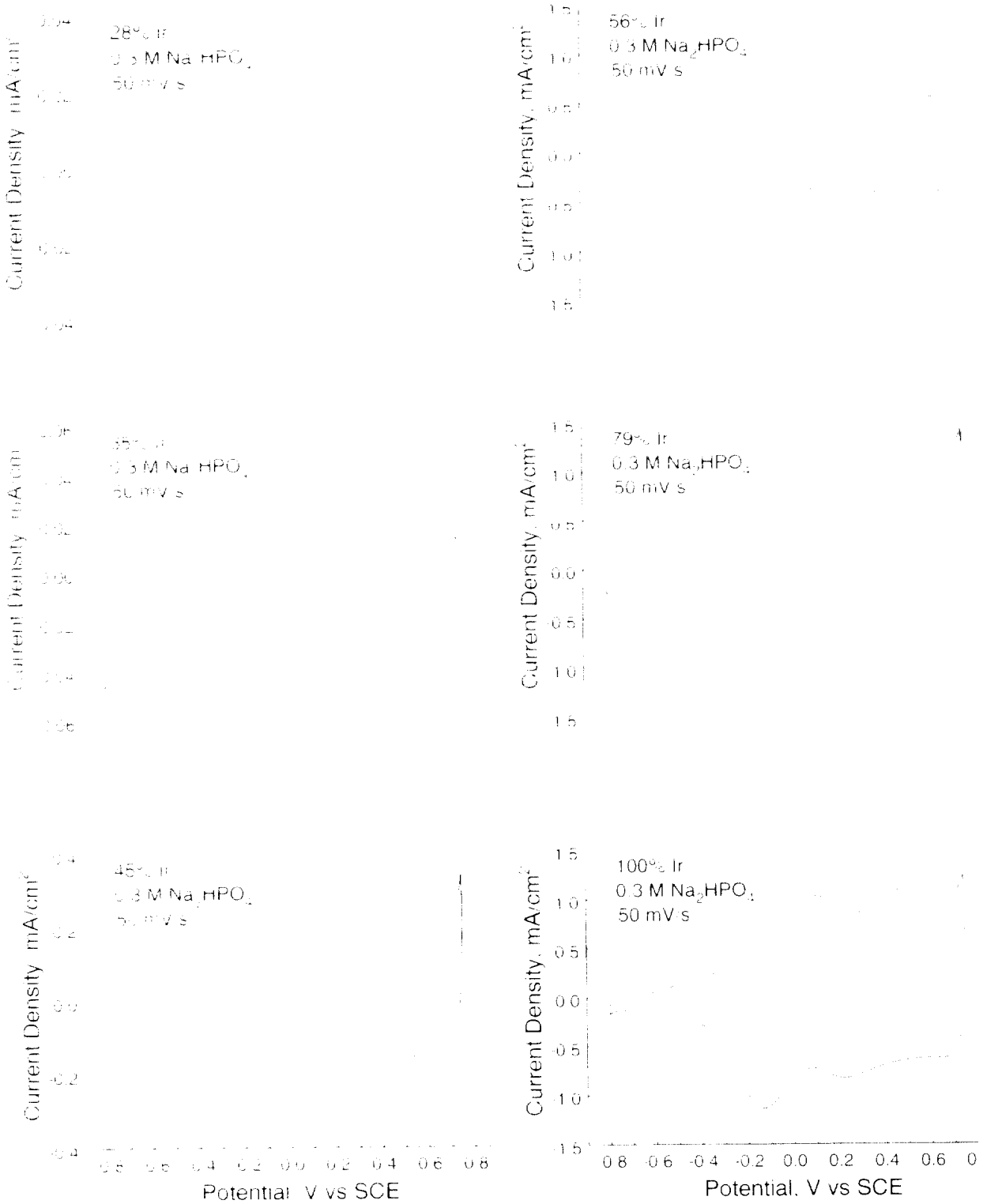


Figure 4-[illegible] Cyclic voltammograms of IrIr alloys following 5,000 pulses in 0.3M $Na_2HPO_4$ between limits of -0.8V and 0.75V vs SCE (note differences in current scale).

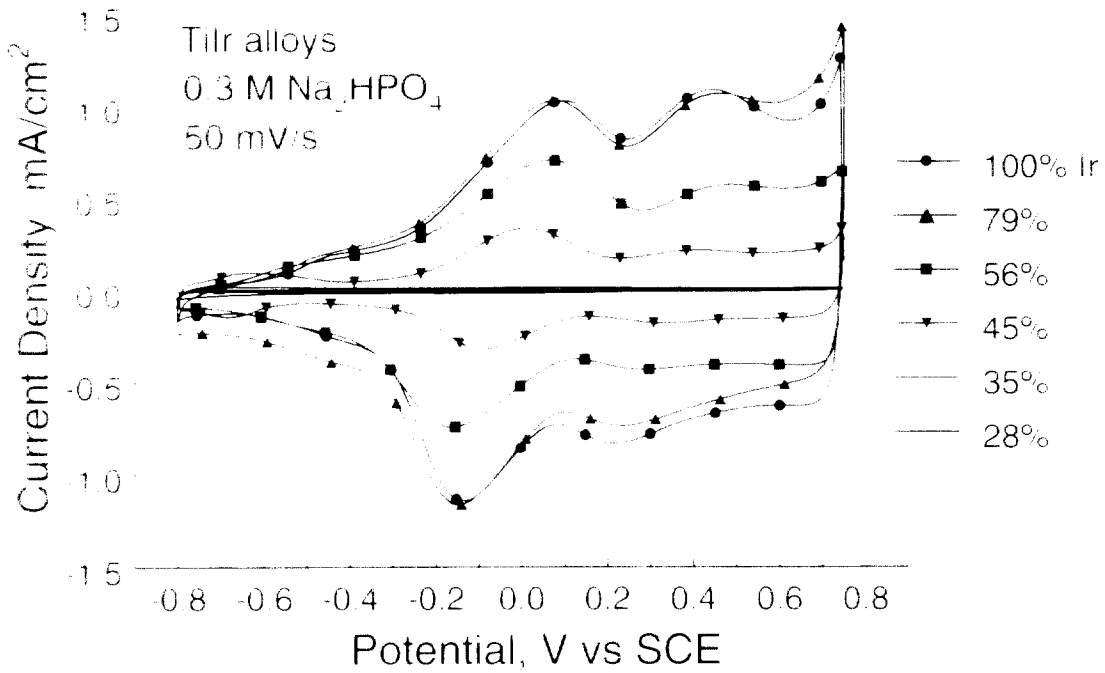


Figure 4-4 Comparison of TiIr alloys following 5,000 pulses in 0.3M $Na_2HPO_4$ between limits of -0.8V and 0.75V vs SCE (see Fig. 4-3). Symbols used for clarity.

Further evaluation of graded interface electrodes will continue in the next reporting period. Activation studies of TiIr alloys are being modified to incorporate longer pulse duration during the activation process to promote more uniform growth of AIROF. Several compositional profiles of graded interface electrodes have been prepared and their stability under overactivation pulsing is being evaluated. Additional SEM work on measuring the volume changes on activation is also underway.

## 6. REFERENCES


1. Burke, L. D., and D. P. Whelan, "A Voltammetric Investigation of the Charge Storage Reactions of Hydrous Iridium Oxide Layers," *J. Electroanal. Chem.*, vol. 166, 121-141, 1984.

2. Yuen, M. F., J. Lauks, and W. C. Dautremont-Smith, "pH dependent voltammetry of iridium oxide films," *Solid State Ionics*, vol. 11, pp. 19-29, 1983.

3. D. B. McCreery, W. F. Agnew, T. G. H. Yuen and L. Bullara, IEEE Trans. Biomed. Eng., **37**, (1990) 996.

4. D. B. McCreery, W. F. Agnew, T. G. H. Yuen and L. Bullara, HMRI Quarterly Progress Report Q1 (1983) Contract NOT-NS-0-2317.

5. J. M. Twardoch, J. Appl. Electrochem. **24** (1994) 835.

6. S. H. Glarum and J. H. Marshall, J. Electrochem. Soc., **127** (1980) 1457.

7. W. Weppner and R. A. Huggins, J. Electrochem. Soc., **124** (1977) 1569.

8. B. A. Boukamp, Computer Program "EQUIVCRT", The computer assisted electrochemical ac-immittance data analysis system, University of Twente, 1988.